ap

Asian Journal of Physics
Vol. 27, No 5 (2018) 257-263
Available on: www.asianjournalofphysics.in

Raman spectroscopy of interlayer vibrational modes in AB-stacked and twisted multilayer graphenes

Miao-Ling Lin[1, 2] and Ping-Heng Tan[1, 2,*]

[1]*State Key Laboratory of Superlattices and Microstructures, Institute of Semiconductors, Chinese Academy of Sciences, Beijing 100083, China*

[2]*CAS Center of Excellence in Topological Quantum Computation, and College of Materials Science and Opto-Electronic Technology, University of Chinese Academy of Sciences, Beijing 100049, China*

The interlayer coupling in multilayer graphenes (MLGs) can be tuned by various stacking configurations, such as common AB-stacking, ABC-stacking and even the twisted multilayer graphene (tMLG). The interlayer shear and breathing coupling can be probed by the interlayer shear (C) modes and layer breathing (LB) modes. Here we first revealed the interlayer shear coupling in MLG by the C modes. In tMLG, the C and LB modes are detected by resonant Raman spectroscopy. The shear interlayer coupling at the interface are 20% of the coupling in the AB-stacked layers, whereas the LB coupling at the interface is similar to that between the AB-stacked layers. This is because that the periodicity mismatch between two twisted layers mostly affects shear interactions. The different couplings for C and LB modes at the interface of tMLG provides a way to identify the layer number of the constituents and the total layer number of tMLG, respectively, which open the doors to identifying the stacking configurations of MLG grown by chemical vapor depositions.

Keywords: Shear modes; Layer breathing modes; interlayer coupling; multilayer graphene; twisted multilayer graphene

1 Introduction

The quest for materials capable of realizing next-generation nanoscale electronic and photonic devices has continued to fuel researches on the electronic [1,2], optical [3] and vibrational properties [4,5] of monolayer graphene (1LG) since the 1LG were firstly extracted from the graphite by micro-mechanical cleavage in 2004 [6]. The near-ballistic transport and high mobility [7], optical transparency [8], quantum hall effect [1], flexibility and environment stability [3,9] of 1LG have intrigued much interests. These fancy properties can also extend to multilayer graphenes (MLGs) [10], which are formed by "combining" 1LG together with defined stacking configurations, such as the common AB-stacking and ABC-stacking. The AB-stacked MLGs (AB-MLGs) exhibit tunable physical properties by varying the layer number [11-16]. For example, bilayer graphene (2LG) is a tunable band gap semiconductors while the trilayer graphene (3LG) has a unique electronic structure consisting of massless 1LG and massive 2LG subband [17]. Besides, by assembling two 1LGs or AB-MLGs with a relative orientation, various homojunction and heterostructures can be formed, which are known as twisted MLG (tMLG). This has raised the possibilities to design the heterostructures and the related devices with demand properties by the interlayer coupling in terms of layer thickness, constituent choices and relative angles [18-23]. In all these graphene-based materials, the graphene layers are stacked with the weak van der Waals coupling since the interlayer distance is much larger than the distance between two adjacent atoms in plane. The ability to probe the interlayer coupling in graphene-

Corresponding author :
e-mail: phtan@semi.ac.cn (Ping-Heng Tan)
The article is based on the lecture deliverd by Ping-Heng Tan at International Conference on Spectroscopy of Biomolecules and Advanced Materials, Oct 4,-7, 2017, at Hotel Haweli, Alappuzha, India

based materials and its impact on the electronic band structure and lattice dynamics is essential to reach a fundamental understanding of these systems. Raman spectroscopy is one of the most used characterization techniques in carbon science and technology [4,5]. There are two fundamental sets of Raman peaks in MLG [15]. The Raman peaks at high wavenumber, such as D, G and 2D, originate from the in-plane vibrations and are also emerged in 1LG. Others at low wavenumber (5~150 cm^{-1}), known as the shear (C) modes and layer breathing (LB) modes, are due to the relative motions of the planes themselves, which are perpendicular or parallel to their normal, respectively [15,21,22]. The detection of the C and LB modes allows one to directly probe the interlayer interactions in AB-MLGs and tMLGs. Here, we firstly uncover the C modes in AB-MLG ranging from 2LG to bulk graphite and gained the interlayer coupling in AB-MLG by the linear chain model [15]. The C and LB modes in tMLG can be directly probed by the resonant Raman spectroscopy since they can be significantly enhanced in resonance with the new optically allowed electronic transitions determined by the relative orientation of the two adjacent layers at the interface. The interlayer coupling at the interface for C modes is revealed to be 20% of the coupling in the AB-MLG while the coupling between layers next to the interface decreases by 9% of that in AB-MLG, due to the periodicity mismatch between the two layers at interface. However, the LB modes are slightly affected by the twisting [22]. Thus, the peak positions of C and LB modes are dependent on the layer number of the constituents and total layer number of tMLG, respectively. This provides way to identify the stacking configuration of CVD-grown MLGs.

2 Shear vibrations in AB-MLG

In order to take insight into the interlayer vibrations in AB-MLG, we firstly consider the Raman modes of 1LG and bulk graphite. There are two atoms in the unit cell of 1LG, resulting in six normal modes at the Brillouin center Γ: $A_{2u}+B_{2g}+E_{1u}+E_{2g}$. There are two degenerate and Raman-active in-plane optical modes, E_{2g} and one Raman-inactive out-of-plane optical mode, B_{2g}. For the unit cell of bulk graphite, there are four atoms, in which the two atoms in each layer are inequivalent. Thus, all optical modes in 1LG become Davydov doublets, E_{2g} generates an infrared-active E_{1u} mode and a Raman-active E_{2g}, whereas the B_{2g} mode divides into an infrared-active A_{2u} mode and a silent B_{2g} mode. The zone boundary acoustic Raman modes are folded on to the zone center and become optical modes: a Raman active E_{2g} and a Raman-inactive mode B_{2g}. Both these two modes are at low wavenumbers due to the relative motions of the rigid plane, either perpendicular or parallel to their normal, which are usually named as C mode and LB mode. When focusing on these two interlayer vibration modes, the graphene layer can be considered as a single ball, and their frequencies are directly dependent on the layer number, interlayer shear and breathing coupling. This is also the case in AB-MLG with layer number N (AB-NLG). Thus, the linear chain model (LCM) can be applied to reproduce the frequencies of C and LB modes in AB-NLG [5,15]

$$\omega(C_{N\,N-i}) = \frac{1}{\pi c}\sqrt{\alpha_0^{\parallel}/\mu}\,\sin(i\pi/2N) \tag{1}$$

$$\omega(LB_{N\,N-i}) = \frac{1}{\pi c}\sqrt{\alpha_0^{\perp}/\mu}\,\sin(i\pi/2N) \tag{2}$$

where $\alpha_0^{\parallel}$, $\alpha_0^{\perp}$ are the interlayer shear and breathing couplings, respectively, μ is the monolayer mass per unit area, i =1,2,...,N–1. For bulk graphite, $N \to \infty$, $\omega(C_{Bulk}) = \frac{1}{\pi c}\sqrt{\alpha_0^{\parallel}/\mu}\,\sin(i\pi/2N)$ and $\omega(LB_{Bulk}) = \frac{1}{\pi c}\sqrt{\alpha_0^{\perp}/\mu}$, which are $\sqrt{2}$ times as much as $\omega(C_{21})$ and $\omega(LB_{21})$, respectively. As measured in experiment, $\omega(C_{Bulk})$ is at 43.5 cm^{-1} [15], while $\omega(LB_{Bulk})$ was estimated as ~125.3 cm^{-1}. So the force constant for layer shear and breathing coupling are $\alpha_0^{\parallel}$=12.8×10^{18} Nm^{-3} and $\alpha_0^{\perp}$ =110.8×10^{18} Nm^{-3}, respectively. Therefore, Eqs (1, and 2) can be simplified as follows:

$$\omega(C_{N\,N-i}) = \omega(C_{Bulk})\,\sin(i\pi/2N) \tag{3}$$

$$\omega(LB_{N\,N-i}) = \omega(LB_{Bulk})\,\sin(i\pi/2N) \quad (4)$$

With these two equations and the frequencies of C and LB modes in graphite, the frequencies of all the C and LB modes for each AB-NLG can be gained. In addition, the normal mode displacements corresponding to each C and LB modes can be also given by solving the $N\times N$ dynamical matrix and thus the symmetry and Raman activity of the C and LB modes can be deduced [5,15].

To explore the C modes in AB-NLG, we firstly check the C mode in AB-2LG. Since both the C and LB modes are at the low wavenumber, a special configuration with three Brag Grate notch filters should be utilized. Here, all the Raman spectra were measured in back scattering geometry using a Jobin-Yvon HR800 Raman system equipped with a liquid nitrogen cooled charge-coupled detector (CCD). The laser excitation is 633 nm from a He–Ne laser with power lower than 0.5 mW in order to prevent the laser heating. The laser plasma lines are removed using a Brag Grate bandpass filter (BPFs) from Opti Grate Corp. and the Rayleigh line is suppressed using three Brag Grate notch filters (BNFs, Opti Grate Corp.) with an optical density 3 (OD = 3) and a spectral bandwidth ~5-10 cm^{-1} [15]. A×100 objective with NA = 0.90 and an 1800 lines per mm grating were used, enabling 0.35 cm^{-1} per pixel of CCD. With this configuration, the signal down to ~5 cm^{-1} can be gained. Recently, the ultralow-frequency Raman measurements at 488 nm excitation down to 2 cm^{-1} approaching the Brillouin scattering regions were accessible by using the BNFs with narrow spectral bandwidth and high optical density (OD > 4) [27]. In the meanwhile, the AB-NLG flakes used in this work were exfoliated from the bulkgraphite onto the SiO_2/Si substrate and the layer number of these samples were characterized by the optical contrast and Raman spectroscopy [16,28].

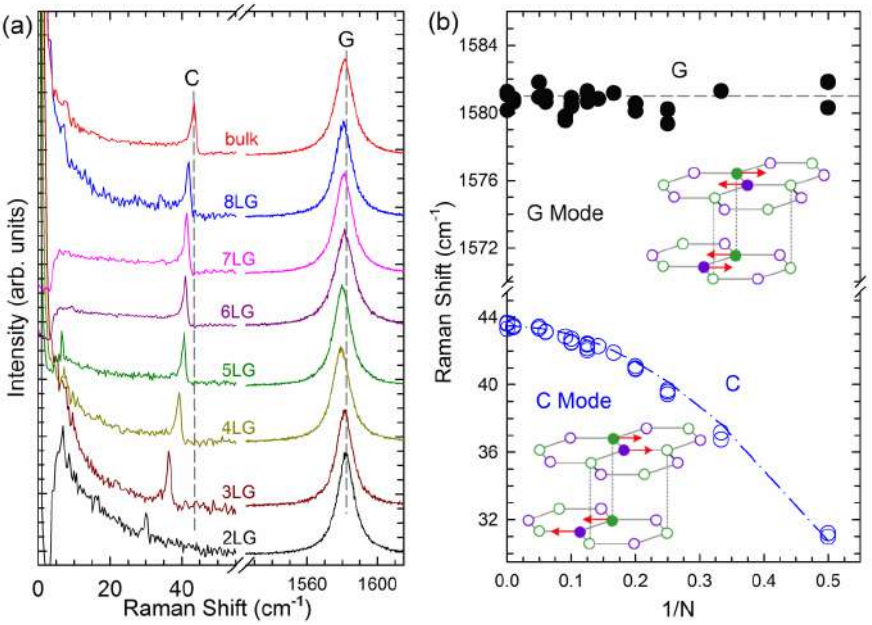

Fig 1. (a) Stokes Raman spectra of the C peak (left) and G peak (right) for AB-stacked 2–8LG and bulk graphite. (b) The position of the G peak (filled black circles) and C peak (open blue circles) as a function of inverse number of layers. The red dashed-dotted line was calculated by LCM. The insets show the atomic displacements of the C and G modes. The vertical dashed lines in (a) and the horizontal line in (b) are eye guides. Reproduced with permission from ref. 15. Copyright 2012, Nature Publishing Group.

Using the technology addressed above, we observed a weak peak at 31 cm^{-1} in 2LG, which is exactly $1/\sqrt{2}$ of that (43.5 cm^{-1}) in bulk graphite [15]. This is in good agreement with the results from LCM.

We also measured the C peak for other AB-*N*LG with *N* ranging from 3 to bulk, as shown in Fig. 1. All the observed C peaks are assigned as C_{N1}. The peak positions of the G modes are almost independent with the layer number. However, the C mode decreases from 43.5 cm^{-1} of bulk graphite to 31 cm^{-1} of bilayer graphene. The frequencies of all C_{N1} modes in AB-*N*LG can be fitted with the same force constant in the equation of LCM, indicating that the interlayer coupling between two graphene layers remain a constant in AB-*N*LG.

It should be noted here that the layer-number dependent LB modes are not emerged in the Raman spectra, which are attributed to the Raman-inactivity or weak electron-phonon coupling. However, the LB modes can be detected by laser heating [29] or combination modes [30,31].

3 Shear and layer breathing vibrations in twisted MLG

Besides the AB stacking for MLG, there also exist other stacking ways, such as ABC and AA stackings. Furthermore, we can assemble the *m*LG and *n*LG with a relative orientation to obtain twisted (*m*+*n*+...)LG. Here, each "+" means one twist interface and the *m*LG, *n*LG are in AB stacking if *m*, *n* >1. Indeed, the *t*(*m*+*n*) LGs ($m \neq n$), exhibit C_3 symmetry and all the C and LB modes are Raman-active. However, the *t*(*n*+*n*) (*n* >1) has D_3 symmetry where the A_2 mode is Raman-inactive and other modes are Raman-active [22]. For example, in *t*(2 + 2)LG, only LB_{42} is Raman-active.

A *t*(1+1)LG and *t*(1+3)LG are selected to be the prototype to reveal the C and LB modes and thus the interlayer coupling in tMLG, in which the 1LG are randomly folded onto the 1LG and 3LG. Since the top graphene layer of *t*(1+1)LG and *t*(1+3)LG is the same layer and the bottom layer is also the same, the twist angle is the same for these two samples. Indeed, the *R* and *R'* modes originated from the TO and LO phonons selected by the twisted wave vector are almost the same. The twist angle for these two samples is determined as 10.6° by the frequencies of *R* and *R'* modes. Furthermore, their optical contrast is quite different from the AB-2LG and AB-4LG, indicating that the band structure of tMLG with layer number *N* (*t*N LG) is modified from those of corresponding AB-*N*LG because of the change of interlayer coupling at the interface.

We measured the Raman spectra in the C peak region for 1LG, 3LG, *t*(1+1)LG and *t*(1+3)LG. There is no C peak in 1LG but one C mode in 3LG, in good agreement with the shear modes in AB-*N*LG addressed above [15]. However, there are no modes at low wavenumber region in *t*(1+1)LG but two modes in *t*(1+3) LG. Their intensity is dependent on the laser wavelength which will discuss below. Since the *t*(1+3)LG is a four-layer graphene, three shear modes are expected. However, the observed frequencies are smaller than the ones of 4LG, but close to those of 3LG [15]. It means that the observed C modes originate from the C modes of three-layer graphene in twisted four layered graphene. Besides, we observed one LB mode in *t*(1+1)LG whose frequency is close to the LB_{21} mode. For *t*(1+3)LG, we observed two modes with frequencies close to the LB_{41} and LB_{42} modes in 4LG. This implies that the frequencies of LB modes are dependent on the total layer number of tMLG. The various tMLG with different constituents are also measured to reveal the C and LB modes and also the interlayer coupling in the twisted systems. The observed C modes in *t*(*m*+*n*)LG with total number of *N* always follow those of the AB-*m*LG and AB-*n*LG (if *m*,*n* >1) constituents, whereas the LB modes always follow those of AB-*N*LG, as shown in Fig 2. To understand the interlayer shear and breathing coupling in *t*(*m*+*n*)LG, we use the LCM as addressed above. Since all the C modes are localized in the constituents of *t*(*m*+*n*)LG, the force constant at the twisted interfaces ($\alpha_t^{\parallel}$) and that between the layers adjacent to the interface ($\alpha_{0t}^{\parallel}$) are considered different from that in AB stacking. Based on the frequencies of C modes in *t*(2+2)LG, *t*(1+3)LG and *t*(2+3)LG, α_t, α_{0t} are estimated as 20% and 91% of that between AB-stacked graphene layers [21]. Similar to the C modes, we fitted the LB modes in *t*(*m*+*n*)LG by LCM with modified interface coupling ($\alpha_t^{\perp}$) and it is estimated to be close to that between AB-stacked graphene layers. However, the large deviation of the frequencies of LB_{N2} in *t*(*m*+*n*)LG suggests that the interlayer breathing force constant between the second-nearset neighbor layers ($\beta_t^{\perp}$) is necessary to reproduce the frequencies of

all the LB modes in $t(m+n)$LG. The new model is denoted as 2LCM and $\beta_t^{\perp}$ is ~9% of that in AB stacking [22].

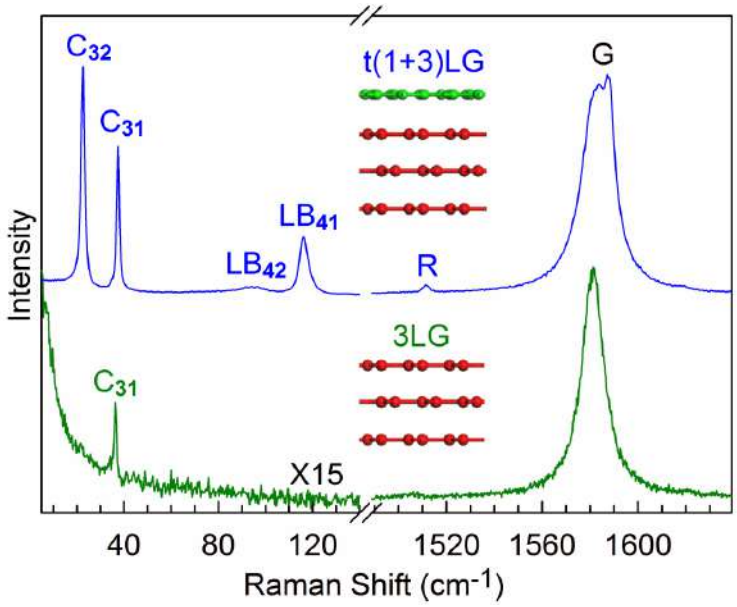

Fig 2. Raman spectra of AB-3LG and t(1+3) LG in the region of C, LB, G peak.

Indeed, for all the tMLG, the C and LB modes can only be observed in a small excitation energy window. When the excitation energy is out of this window, the C and LB modes are absent. The enhancements of C and LB modes in the resonant window originate from the new optically-allowed transition in tMLG, which are strongly dependent on the twist angle. Thus, using the resonant Raman spectroscopy, the observed C modes can be used to identify the layer number of the AB-stacked constituents while the LB modes can be used to distinguish the total layer number in tMLG.

4 The Characterisation of Stacking Configurations of CVD-Grown MLG

Based on the different shear and breathing couplings in MLG, the interlayer vibrations can be utilized to characterize the stacking configurations of MLG, especially for those grown by CVD [32].The CVD-grown 2LG tends to produce twisted 2LG (t2LG), in which one monolayer sheet rotates by a certain angle (ϑ) relative to the other. Similarly, the NLG can exhibit AB stacking or twisted stacking. For the MLG with a given total layer number N (with $N = n+m+...$), there may exist up to $N - 1$ twisted interfaces. Therefore, the stacking configurations of NLG become more and more complicated with increasing NLG. Once an additional layer is added to the NLG, AB-stacked or twisted interface is alternatively formed relative to the adjacent layer. With this tendency, there should be $(2N–1)$ kinds of stacking configurations in NLG. For example, the number of stacking configurations for 3LG is four: AB-3LG, t(1+2)LG, t(2+1)LG and t(1+1+1) LG. In this case, the stacking configurations of tNLG can be figured out once the total number of tNLG, the layer number of the AB-stacked constituents of tNLG and the twist angle at the interface are determined. Here we measured the Raman spectra in the region of C, LB and G peak layer by layer. As addressed above, the LB modes are helpful to distinguish the total layer number of NLG while the layer number of AB-stacked constituents are accessible by the C modes. With this method, the stacking sequences of each flakes can be figured out by the interlayer vibrations. In addition, the ϑ at the interface can be determined by the so-called R and R' modes originating from the TO and LO phonons selected by the twisted wave vector. This paves the

way to characterizing the stacking configurations of CVD-MLG for fundamental research and for optimizing experimental conditions to grow CVD-MLG with specific stacking configurations.

5 Conclusions

To sum up, we uncover the C modes in AB-stacked MLG and determine the interlayer coupling by fitting the frequencies of C modes by the LCM. Furthermore, the C and LB modes of tMLG are ascertained using the resonant Raman spectroscopy since they can be significantly enhanced when the excitation energy approaches the new twist-angle dependent optical-allowed transitions. The C modes are revealed to locate in the AB-stacked constituents of tMLG while the LB modes are from the collective motions of all the stacked layers. With the modified LCM, the interlayer shear coupling at the interface is only about 20% of that in AB stacking while the coupling for LB modes change slightly. According to the behavior of C and LB modes in tMLG, they can be utilized to characterize the stacking configurations of CVD-MLG. This provides the way to use Raman spectroscopy to uncover the interface coupling of two-dimensional hybrids and heterostructures.

Acknowledgments

We acknowledge support from the National Key Research and Development Program of China (Grant No.2016YFA0301204), the National Natural Science Foundation of China (Grant No. 11474277 and 11434010), and Beijing municipal Science and technology commission.

References

1. Novoselov K S, Geim A K, Morozov S V, Jiang D, Katsnelson M I, Grigorieva I V, Dubonos S V, Firsov A A, *Nature*, 438(2005)197-200.
2. Lin Y.-M, Dimitrakopoulos C, Jenkins K A, Farmer D B, Chiu H.-Y, Grill A, Avouris P, *Science*, 327(2010)662; doi: 10.1126/science.1184289.
3. Bonaccorso F, Sun Z, Hasan T, Ferrari A C, *Nat Photon*, 4(2010)611-622.
4. Ferrari A C, Basko D M, *Nat Nanotechnol*, 8(2013)235-246.
5. Wu J.-B, Lin M.-L, Cong X, Liu H.-N, Tan P.-H, *Chem Soc Rev*, 47(2018)1822-1873.
6. Novoselov K S, Geim A K, Morozov S V, Jiang D, Zhang Y, Dubonos S V, Grigorieva I V, Firsov A A, *Science*, 306(2004)666-669.
7. Morozov S V, Novoselov K S, Katsnelson M I, Schedin F, Elias D C, Jaszczak J A, Geim A K, *Phys Rev Lett*, 100(2008)016602; doi.org/10.1103/PhysRevLett.100.016602
8. Nair R R, Blake P, Grigorenko A N, Novoselov K S, Booth T J, Stauber T, Peres N M R, Geim A K, *Science*, 320 (2008)1308; doi: 10.1126/science.1156965
9. Geim A K, Novoselov K S, *Nature Materials*, 6(2007)183-191.
10. Zhu W, Perebeinos V, Freitag M, Avouris P, *Phys Rev B*, 80(2009)235402; doi.org/10.1103/PhysRevB.80.235402.
11. Guinea F, Neto A H Castro, Peres N M R, *Phys Rev B*, 73(2006)245426; doi.org/10.1103/PhysRevB.73.245426
12. Taychatanapat T, Watanabe K, Taniguchi T, Jarillo-Herrero P, *Nature Phys*, **7**(2008)621-625.
13. Lui C H, Li Z, Chen Z, Klimov P V, Brus L E, Heinz T F, *Nano Lett*, 11(2011)164-169.
14. Ye J, Craciun M F, Koshino M, Russo S, Inoue S, Yuan H, Shimotani H, Morpurgo A F, Iwasa Y, *Proc Natl Acad Sci USA*, 108(2011)13002-13006.
15. Tan P.-H, Han W.-P, Zhao W.-J, Wu Z.-H, Chang K, Wang H, Wang Y.-F, Bonini N, Marzari N, Pugno N, Savini G, Lombardo A, Ferrari A C, *Nat Mater*, 11(2012)294-300.
16. Li X.-L, Han W.-P, Wu J.-B, Qiao X.-F, Zhang J, Tan P.-H, *Adv Funct Mater 27*, (2017)1604468; doi.org/10.1002/adfm.201604468
17. Mikito K, Tsuneya A, *Solid State Commun*, 149(2009)1123-1127.

18. Li G, Luican A, Santos J M B Lopes dos, Neto A H Castro, Reina A, Kong J, Andrei E Y, *Nat Phys*, 6(2010) 109-113.
19. Lee D S, Riedl C, Beringer T, Neto A H Castro, von Klitzing K, Starke U, Smet J H, *Phys Rev Lett*, 107(2011) 216602; doi.org/10.1103/PhysRevLett.107.216602
20. Morell E S, Pacheco M, Chico L, Brey L, *Phys Rev B*, 87(2013)125414; doi.org/10.1103/PhysRevB.87.125414
21. Wu J.-B, Zhang X, Ijas M, Han W.-P, Qiao X.-F, Li X.-L, Jiang D.-S, Ferrari A C, Tan P.-H, *Nat Commun*, 5(2014)5309.
22. Wu J.-B, Hu Z.-X, Zhang X, Han W.-P, Lu Y, Shi W, Qiao X.-F, M. Ijiäs M, Milana S, Ji W, Ferrari A C, Tan P.-H, *ACS Nano*, 9(2015)7440-7449.
23. Eliel G S N, Moutinho M V O, Gadelha A C, Righi A, Campos L C, Ribeiro H B, Chiu P.-W, Watanabe K, Taniguchi T, Puech P, Paillet M, Michel T, Venezuela P, Pimenta M A, *Nat Commun*, 9(2018)1221; doi: 10.1038/s41467-018-03479-3.
24. Ferrari A C, Robertson J, *Philos Transact. A Math Phys Eng Sci*, 362(2004)2477; doi: 10.1098/rsta.2004.1452
25. Zhang X, Han W-P, Wu J-B, Milana S, Lu Y, Li Q Q, Ferrari A C, Tan P-H, *Phys Rev B*, 87(2013)115413; doi.org/10.1103/PhysRevB.87.115413
26. Zhang X, Qiao X-F, Shi W, Wu J-B, Jiang D S, Tan P-H, *Chem Soc Rev*, 44(2015)2757-2785.
27. Liu X.-L, Liu H.-N, Wu J.-B, Wu H.-X, Zhang T, Zhao W.-Q, Tan P.-H, *Rev Sci Instrum*, 88(2017)053110; doi.org/10.1063/1.4983144
28. Ferrari A C, Meyer J C, Scardaci V, Casiraghi C, Lazzeri M, Mauri F, Piscanec S, Jiang D, Novoselov K S, Roth S, Geim A K, *Phys Rev Lett*, 97(2006)187401; doi:10.1103/PhysRevLett.97.187401 .
29. Lui C H, Ye Z, Keiser C, Xiao X, He R, *Nano Lett*, 14(2014)4615-4621.
30. Herziger F, May P, Maultzsch J, *Phys Rev B*, 85(2012)235447; doi.org/10.1103/PhysRevB.85.235447
31. Lin M.-L, Wu J.-B, Liu X.-L, Tan P.-H, *J Raman Spectrosc*, 49(2018)19-30.
32. Lin M.-L, Chen T, Lu W, Tan Q.-H, Zhao P, Wang H.-T, Xu Y, Tan P.-H, *J Raman Spectrosc*, 49(2018)46-53.

[*Received*: 1.4.2018; *revised recd*: 29.5.2018; *accepted*:30.5.2018]

Ping-Heng Tan

Ping-Heng Tan is a Professor at Institute of Semiconductors, Chinese Academy of Sciences. He obtained his B.S. at Peking University and completed his Ph.D. at Chinese Academy of Sciences. His current research focuses on the optical properties of two-dimensional layered materials. He has published over 160 peer-reviewed papers in scientific international journals. Some of them have been published in Nature Materials, Nature Communications, Chemical Society Review and Physical Review Letters. He was supported by NSFC for Distinguished Young Scholars in 2012 and was awarded Huang Kun prize in Physics in 2015. Now, he is the Editorial Board members of "Journal of Raman Spectroscopy", "Semiconductor Science and Technology", and "npj 2D Materials and Applications". Recetly he has joined as Editor Asian J Phys. During International Conference on Spectroscopy of Biomolecules and Advanced Materials, Oct 4,-7, 2017, at Hotel Haweli, Alappuzha, he was awarded 1st Dayawati Rastogi Lecture Award.

Miao-Ling Lin

Miao-Ling Lin received her BS (2014) in physics from Nankai University, Tianjin, China. She is now a Ph D student supervised by Prof. Ping-Heng Tan in the State Key Laboratory of Superlattice and Microstructures, Institute of Semiconductors, Chinese Academy of Sciences. Her current research interest focuses on optical properties of low-dimensional nanomaterials.

linmiaoling@semi.ac.cn